Article:
(2019) Nuclear structure of Ni 76 from the (p,2p) reaction. Physical Review C. 014312. ISSN 2469-9993

https://doi.org/10.1103/PhysRevC.99.014312

Nuclear structure of ^{76}Ni from the $(p, 2p)$ reaction

Z. Elekes,[1] Á. Kripkó,[1] D. Sohler,[1] K. Sieja,[2] K. Ogata,[3,4] K. Yoshida,[5] P. Doornenbal,[6] A. Obertelli,[6,7,8] G. Authelet,[8] H. Baba,[6] D. Calvet,[8] F. Château,[8] A. Corsi,[8] A. Delbart,[8] J.-M. Gheller,[8] A. Gillibert,[8] T. Isobe,[6] V. Lapoux,[8] M. Matsushita,[9] S. Momiyama,[10] T. Motobayashi,[6] H. Otsu,[6] C. Péron,[8] A. Peyaud,[8] E. C. Pollacco,[8] J.-Y. Roussé,[8] H. Sakurai,[6,10] C. Santamaria,[6,8] Y. Shiga,[6,11] S. Takeuchi,[6] R. Taniuchi,[6,10] T. Uesaka,[6] H. Wang,[6] K. Yoneda,[6] F. Browne,[12] L. X. Chung,[13] Zs. Dombrádi,[1] F. Flavigny,[14] S. Franchoo,[14] F. Giacoppo,[15] A. Gottardo,[14] K. Hadyńska-Klęk,[15] Z. Korkulu,[1] S. Koyama,[10] Y. Kubota,[6,9] J. Lee,[16] M. Lettmann,[7] C. Louchart,[7] R. Lozeva,[2,17,18] K. Matsui,[6,10] T. Miyazaki,[10] M. Niikura,[10] S. Nishimura,[6] L. Olivier,[14] S. Ota,[9] Z. Patel,[19] E. Sahin,[15] C. Shand,[19] P.-A. Söderström,[6] I. Stefan,[14] D. Steppenbeck,[9] T. Sumikama,[20] D. Suzuki,[14] Zs. Vajta,[1] V. Werner,[7] J. Wu,[6,21] and Z. Xu[16]

(SunFlower Collaboration)

[1]*MTA Atomki, P.O. Box 51, H-4001 Debrecen, Hungary*
[2]*CNRS, UMR 7178, F-67037 Strasbourg, France*
[3]*Research Center for Nuclear Physics (RCNP), Osaka University, Ibaraki 567-0047, Japan*
[4]*Department of Physics, Osaka City University, Osaka 558-8585, Japan*
[5]*Advanced Science Research Center, Japan Atomic Energy Agency, Tokai, Ibaraki 319-1195, Japan*
[6]*RIKEN Nishina Center, 2-1 Hirosawa, Wako, Saitama 351-0198, Japan*
[7]*Institut für Kernphysik, Technische Universität Darmstadt, 64289 Darmstadt, Germany*
[8]*IRFU, CEA, Université Paris-Saclay, F-91191 Gif-sur-Yvette, France*
[9]*Center for Nuclear Study, University of Tokyo, RIKEN Campus, Wako, Saitama 351-0198, Japan*
[10]*Department of Physics, University of Tokyo, 7-3-1 Hongo, Bunkyo, Tokyo 113-0033, Japan*
[11]*Department of Physics, Rikkyo University, 3-34-1 Nishi-Ikebukuro, Toshima, Tokyo 172-8501, Japan*
[12]*School of Computing Engineering and Mathematics, University of Brighton, Brighton BN2 4GJ, United Kingdom*
[13]*Institute for Nuclear Science & Technology, VINATOM, P.O. Box 5T-160, Nghia Do, Hanoi, Vietnam*
[14]*Institut de Physique Nucléaire, IN2P3-CNRS, Université Paris-Sud, Université Paris-Saclay, 91406 Orsay Cedex, France*
[15]*Department of Physics, University of Oslo, N-0316 Oslo, Norway*
[16]*Department of Physics, The University of Hong Kong, Pokfulam, Hong Kong*
[17]*Université de Strasbourg, IPHC, 23 rue du Loess, F-67037 Strasbourg, France*
[18]*CSNSM, CNRS/IN2P3, Université Paris-Saclay, F-91405 Orsay Campus, France*
[19]*Department of Physics, University of Surrey, Guildford GU2 7XH, United Kingdom*
[20]*Department of Physics, Tohoku University, Sendai 980-8578, Japan*
[21]*State Key Laboratory of Nuclear Physics and Technology, Peking University, Beijing 100871, People's Republic of China*

(Received 28 August 2018; revised manuscript received 19 November 2018; published 14 January 2019)

The nuclear structure of the ^{76}Ni nucleus was investigated by $(p, 2p)$ reaction using a NaI(Tl) array to detect the deexciting prompt γ rays. A new transition with an energy of 2227 keV was identified by $\gamma\gamma$ and $\gamma\gamma\gamma$ coincidences. According to these coincidence spectra the observed transition connects a new state at 4147 keV and the previously known 4_1^+ state at 1920 keV. Two weaker transitions were also obtained at 2441 and 2838 keV, which could be tentatively placed to feed the known 2_1^+ state at 990 keV. Our shell-model calculations using the Lenzi, Nowacki, Poves, and Sieja interaction produced good candidates for the experimental proton hole states in the observed energy region, and the theoretical cross sections showed good agreement with the experimental values. Although we could not assign all the experimental states to the theoretical ones unambiguously, the results are consistent with a reasonably large $Z = 28$ shell gap for nickel isotopes in accordance with previous studies.

DOI: 10.1103/PhysRevC.99.014312

I. INTRODUCTION

Since the discovery of magic neutron and proton numbers in stable nuclei and the seminal works by Maria Göppert–Mayer on the interpretation of this structural property by the nuclear shell model [1,2], scientists have been interested in whether the location of single-particle states and the magic numbers change away from stability. In the past thirty years, by the widespread use of beams of ions with nuclei of exotic neutron-to-proton ratios it has become evident that the magic numbers among extremely-neutron-rich and -proton-rich isotopes may indeed differ from those close to the stability. Extraordinary experimental effort was devoted to uncover this phenomenon especially for the neutron number (N) 20 (see, e.g., Refs. [3–7]). For larger neutron numbers the magicity of

$N = 28$ was also proved to be soft; for example, in the ^{42}Si nucleus [8,9]. Regarding the protons, there are accumulating pieces of evidence for a new magic number at 6 in addition to 8 for neutron-rich carbon isotopes [10]. On the proton-rich side of the nuclear chart there were indications for a new magic number at 16 instead of 20 in the ^{28}S nucleus [11] as well.

For these structural changes, mainly the Tokyo theoretical group developed an explanation that is connected to the monopole part of the neutron-proton interaction (see, e.g., Refs. [12,13]). This concept was applied for the larger magic numbers, especially for neutron number 50 and proton number (Z) 28 (see, e.g., Refs. [14–17]), which inspired many spectroscopic experiments when this region became available by the radioactive ion beam facilities (see, e.g., Refs. [18–24]) to approach the possibly doubly magic nucleus ^{78}Ni.

Just two neutrons away from ^{78}Ni, the even-even nucleus ^{76}Ni is an ideal candidate to investigate the shell evolution. In particular, the $Z = 28$ shell gap can be surveyed by proton knock-out reactions, so we carried out a γ-spectroscopy experiment via the ^{77}Cu$(p, 2p)^{76}$Ni reaction to explore proton hole states in ^{76}Ni and to investigate the proton shell gap 28. The yrast band of ^{76}Ni up to the 8^+ level is relatively well known from previous studies [18]. In addition to this yrast band, another γ ray was detected in the β decay of the assumed ground state of ^{76}Co [25], tentatively placed to feed the 2_1^+ state. Beyond this we step into terra incognita regarding the low-energy level structure of ^{76}Ni.

II. EXPERIMENT

The experiment was carried out at the Radioactive Isotope Beam Factory (RIBF) maintained by the RIKEN Nishina Center and the Center for Nuclear Study of the University of Tokyo. As a first step to get the radioactive beam, ^{238}U ions were produced by an electron cyclotron resonance ion source and were fed into the linear accelerator RILAC of RIBF. The ions were then further accelerated by the four coupled cyclotrons of RIBF, RRC, fRC, IRC, and SRC, ending up with a beam energy of 345 MeV/nucleon and a beam intensity of 12 pnA. The ^{238}U beam was transported to a ^{9}Be primary target with a thickness of 3 mm placed at the entrance of the BigRIPS separator [26] in order to induce in-flight fission. From the produced radioactive isotopes of many different kinds, the constituents of the secondary beam were selected by the $B\rho$-ΔE-$B\rho$ method ($B\rho$ is magnetic rigidity, ΔE is energy loss) using slits and an aluminum wedged degrader at the first focal plane F1, located between the two dipole magnets D1 and D2 of BigRIPS. The different radioactive ions of the resulting cocktail beam were then tagged between focal planes F3 and F7 by time-of-flight (TOF), energy loss, and magnetic rigidity measurements. The TOF was determined by plastic scintillators at F3 and F7, providing a time resolution of about 40 ps [27], while ΔE was yielded by a tilted electrode gas ionization chamber at F7 [28]. The trajectory of the particles was monitored by several sets of parallel plate avalanche counters (PPAC) at F3, F5, and F7 [29,30].

The ^{76}Ni isotopes to be studied were produced through nucleon-removal reactions by using the MINOS device [31], which consisted of a liquid hydrogen target surrounded by a cylindrical time-projection chamber (TPC). The liquid hydrogen with a temperature of 20 K was placed inside a polyethylene terephthalate cell, which had an entrance window diameter and thickness of 38 mm and 110 μm, respectively. The ions left the target through an exit window of 52 mm diameter and 150 μm thickness. The effective target length was measured to be 102(1) mm. The length, the inner diameter and the outer diameter of the TPC were 300, 80, and 178.8 mm, respectively. The TPC chamber was filled with a gas mixture of argon, CF_4, and isobutane at room temperature and atmospheric pressure. The vertex position was reconstructed either by using the scattered and the removed protons or one of the protons and the projected trajectory of the radioactive ions (the former method was preferred when both data were available). An overall efficiency of 95% and a resolution of 5 mm (FWHM) along the beam axis was achieved for the events when at least one proton was recorded by the TPC.

For the detection of prompt γ rays, 186 NaI(Tl) crystals of DALI2 [9] were built around the MINOS device. The arrangement of the scintillators was optimized for total photopeak efficiency and resolution. Therefore, they were packed in 10 cylindrical layers with 10–14 units, while in the forward direction a wall of 64 detectors served to observe the γ rays. The beginning of the liquid hydrogen target was just 8 mm upstream of the edge of the first layer of the DALI2 array. The beam-like heavy ions leaving the target were identified by the ZeroDegree spectrometer [26] operated in large acceptance mode using the same principles applied at BigRIPS [27]. The elements of the ZeroDegree spectrometer were similar to the BigRIPS separator while its length was 36.5 m and included four focal planes (F8, F9, F10, F11) where the beamline detectors were placed to measure the properties of the ions. The TOF was taken between F8 and F11 by plastic scintillators and the ΔE was measured by an ionization chamber at F11. PPACs were applied at F8, F9, and F11 to provide information of the trajectory of the ions. In total 5.5×10^3 particles hit the liquid hydrogen target every second while the intensity of ^{77}Cu ions was only 10 pps. In Fig. 1 the particle identification plot of the incoming ions can be seen incoincidence with outgoing ^{76}Ni ions tagged by the ZeroDegree spectrometer. This shows that the ^{76}Ni ions mainly originated from nucleon removal reactions on ^{81}Ga, ^{79}Zn, ^{80}Zn, ^{77}Cu, ^{78}Cu, ^{79}Cu nuclei, and many unreacted nuclei passed through the target. Figure 2 is also a particle identification plot but with an additional coincidence on protons detected by the MINOS device. The ^{77}Cu$(p, 2p)^{76}$Ni reaction amounted to about 7% of the ^{76}Ni-producing events and occurred at a mean energy of 229 MeV/nucleon.

III. RESULTS AND DISCUSSION

The energy calibration of the DALI2 detectors was done several times during the collection of the data by ^{60}Co, ^{137}Cs, and ^{88}Y radioactive sources. The Doppler correction was performed by using the vertex information from the MINOS TPC. To extract this position information, a tracking algorithm [32] was applied, and the change in the drift velocity during

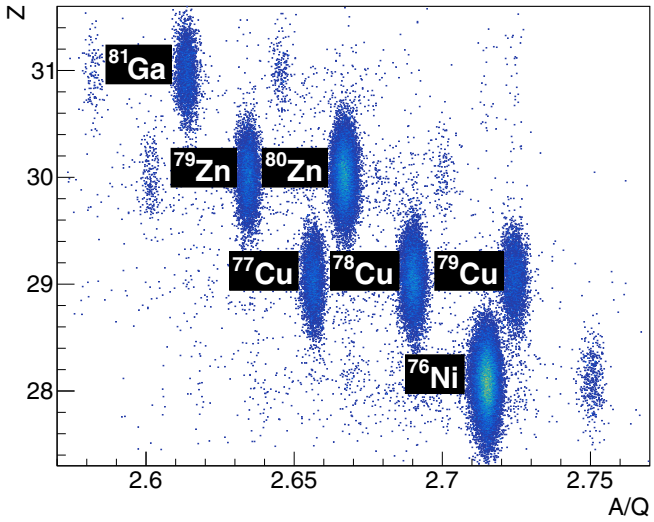

FIG. 1. Particle identification of the incoming cocktail beam in coincidence with outgoing ^{76}Ni ions tagged in the ZeroDegree spectrometer.

the time of the experiment was also taken into account. The efficiency of the DALI2 array was increased by the addback method, which reconstructs the total energy of the γ rays hitting the neighboring NaI(Tl) units, putting the events of Compton scattering and pair production to the photopeak in the γ-ray spectrum.

Figure 3 demonstrates the results for ^{76}Ni. The upper panel shows the singles spectrum. The experimental data are represented by dots with error bars and shaded area. The known transitions with energies of 930 and 990 keV [25] appear in the spectrum as an unresolved peak. However, a small peak around 2.8 MeV is also present as well as a peak-like structure around 2.0–2.5 MeV not observed previously. To investigate the origin of the new peaks, $\gamma\gamma$ and $\gamma\gamma\gamma$ matrices were generated. The middle panel shows a one-dimensional projection of the $\gamma\gamma$ coincidences with an energy cut that corresponds to the peak of $930 + 990$ keV. This clearly shows that the transitions with energies of 930 and 990 keV form a cascade, which is expected from previous studies [18,25,33,34]. The spectrum also provides an even more pronounced high-energy peak structure at around 2.0–2.5 MeV as well as a peak at 2.8 MeV. From the known energy resolution of the setup we can conclude that there must be at least two γ rays involved in the structure around 2.0–2.5 MeV. A high-energy fit with three peaks provides the energy of the transitions to be 2227(35), 2441(50), and 2838(69) keV. The energy uncertainties mainly

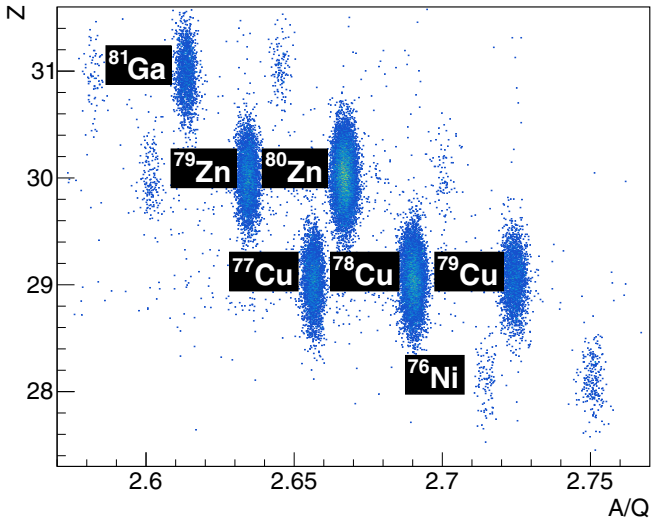

FIG. 2. Particle identification of the incoming cocktail beam in coincidence with outgoing ^{76}Ni ions tagged in the ZeroDegree spectrometer and protons detected in the MINOS device.

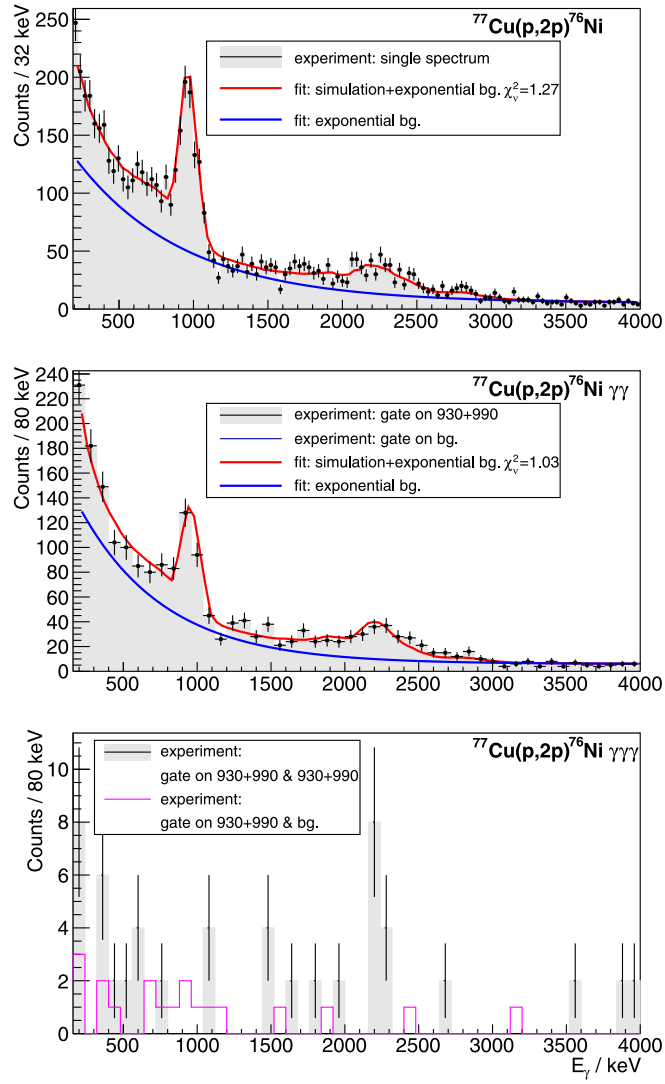

FIG. 3. Doppler-corrected γ ray spectra of ^{76}Ni using vertex reconstruction (requiring only a single proton in the TPC) and addback procedure (upper panel: singles, middle panel: projection of $\gamma\gamma$ coincidences, lower panel: projection of $\gamma\gamma\gamma$ coincidences). The data with error bars and shaded area represent the experimental spectrum, the red line is the simulation plus an exponential background, and the latter function (exponential background) is also plotted separately as a blue line. Magenta stands for spectra of coincidence events ($\gamma\gamma$ and $\gamma\gamma\gamma$) with cuts on the background close to the peaks.

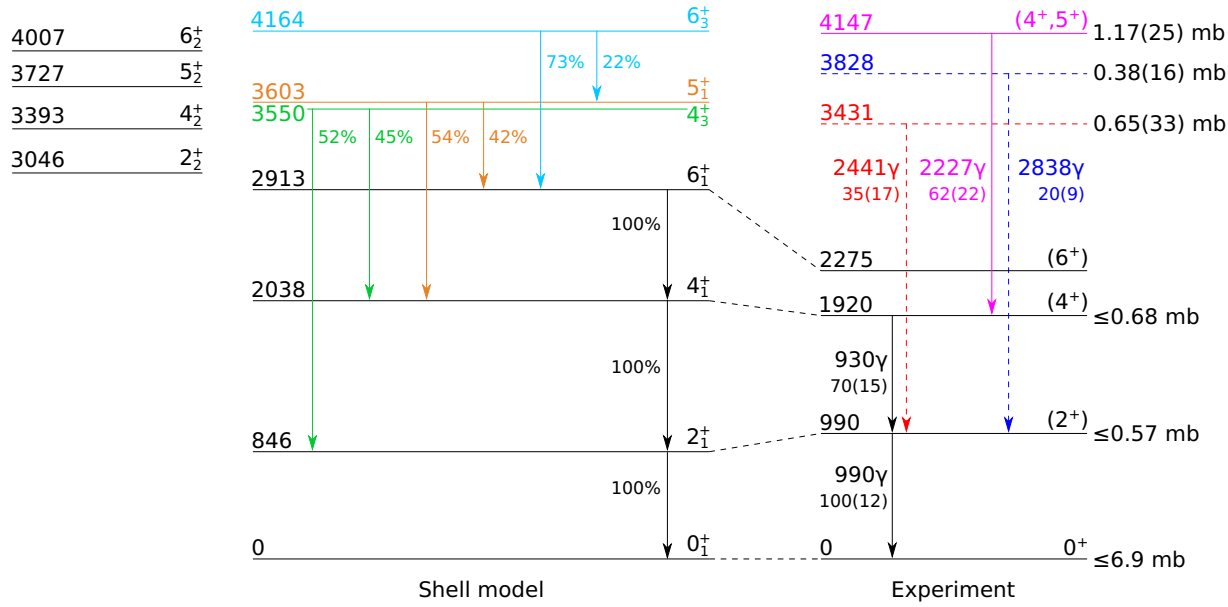

FIG. 4. Partial level and decay scheme of ^{76}Ni showing the two known, lowest-lying transitions with energies of 930 and 990 keV. The newly established proton hole state at 4147 keV (magenta) decaying with a γ ray of 2227 keV to the second-excited state (4_1^+) is also drawn. The two other observed γ rays are tentatively placed to feed the 2_1^+ state, resulting in excited proton hole states at 3431 keV (red) and 3828 keV (blue). The numbers on the right-hand side of the levels indicate the extracted exclusive cross section of the states in the ^{77}Cu$(p, 2p)^{76}$Ni reaction. The experimental data are compared with our shell-model calculations. The three lowest excited levels can be unambiguously matched with the experimental states. The calculation provides four states (2_2^+, 4_2^+, 5_2^+, 6_2^+) associated with mainly neutron excitations in the energy region of the observed states not populated in the $(p, 2p)$ reaction. The colored (green, brown, cyan) theoretical levels are proton hole states that are good candidates for the experimental states.

come from statistics since the uncertainty due to the calibration is just 5 keV. The statistical confidence of the three peaks is 5.5σ, 3.3σ, and 2.3σ, respectively. These transitions are in coincidence with either the transition with an energy of 990 keV or with both the 930 keV and the 990 keV ones. The lower panel in Figure 3 clarifies the situation because it shows a one-dimensional projection of the $\gamma\gamma\gamma$ coincidences with two energy cuts on the unresolved $930 + 990$ keV peak. A peak at around 2.3 MeV also appears in this spectrum, which proves that the transition of 2227 keV forms a cascade with the transitions of 930 and 990 keV, and this new γ ray most probably feeds the known state at 1920 keV (4_1^+). It cannot populate the known state at 2275 keV (6_1^+) because we did not observe a γ ray of 355 keV connecting 6_1^+ and 4_1^+ states (see the discussion on the partial half-life for the 355 keV photon later). The two other new γ rays (2441, 2838 keV) can be tentatively placed to connect new states at 3431 and 3828 keV and the known 2_1^+ state. Probably, they do not populate the 4_1^+ and the 6_1^+ states strongly because we do not observe them in the spectrum of $\gamma\gamma\gamma$ coincidences. The relative intensities of the detected γ rays were deduced to be 100(12)%, 70(15)%, 62(22)%, 35(17)%, and 20(9)% for 990, 930, 2227, 2441, and 2838 keV, respectively.

To check whether the experimental spectra can be matched to the expected response of the DALI2 array using such a γ-ray cascade (right part of Fig. 4), a simulation was performed with the GEANT4 code [35]. The resolution of the DALI2 detectors were adjusted in the simulation to equal the values in the experimental spectra taken with the radioactive sources. The simulation results are represented as red lines in the figures. The blue line in Fig. 3 is an exponential function added to the simulated response in order to mimic the background (originating from unresolved transitions, particles hitting the detectors, and other materials followed by γ emission) present in the experimental spectrum. Magenta is used to show the experimental background spectrum for the coincidence events produced by using energy cuts near the peaks. The inclusive cross section was determined to be 8.4(4) mb, while the exclusive cross sections could be extracted to be 0.65(33) mb for the 3431 keV state, 0.38(16) mb for the 3828 keV state, and 1.17(25) mb for the 4147 keV state. Finally, it could be concluded that the exclusive cross section is $\leqq$6.9 mb for the ground state, $\leqq$0.57 mb for the first excited state and $\leqq$0.68 mb for the second-excited state. In a simple approach, we can suppose that the observed excited states correspond to the multiplet of 1^+–6^+levels created by elevating a proton from $f_{7/2}$ to $f_{5/2}$ orbital across the $Z = 28$ shell gap.

To see how the observed level and decay scheme compares with theory as well as to shed light on the fate of the shell closure $Z = 28$, large-scale shell-model calculations were performed in the valence space comprising neutron ($f_{5/2}p_{1/2}g_{9/2}d_{5/2}$) and proton fp orbitals. The Hamiltonian employed here was the one based on the Lenzi, Nowacki, Poves, and Sieja interaction [36], which was used recently to study the copper isotopes from ^{69}Cu to ^{77}Cu [37–39]. Due

TABLE I. Occupation numbers of proton orbits for the lowest three theoretical states (E_{theor}) and for the strongest proton hole states from our shell-model calculations.

E_{theor}	J^π	Proton orbits			
(MeV)		$f_{7/2}$	$f_{5/2}$	$p_{3/2}$	$p_{1/2}$
0	0_1^+	7.48	0.30	0.19	0.02
0.846	2_1^+	7.48	0.29	0.20	0.02
2.038	4_1^+	7.52	0.28	0.18	0.02
3.550	4_3^+	6.65	0.92	0.32	0.11
3.603	5_1^+	6.63	1.00	0.30	0.07
4.164	6_3^+	6.68	0.97	0.30	0.06

to the large size of the configuration space, the calculations were truncated to $8p$-$8h$ excitations across $Z = 28$ and $N = 40$ gaps, which assured, however, a good convergence of the calculated spectra for ^{76}Ni. The diagonalization of the Hamiltonian matrices was achieved by using the Strasbourg shell-model code ANTOINE [40,41]. To get theoretical branching ratios, the $E2/M1$ reduced transitions rates were obtained by using effective charges $e_p = 1.31$, $e_n = 0.46$ for $B(E2)$ and $g_l^n = -0.1$, $g_s^n = -2.87$, $g_l^p = 1.1$, $g_s^p = 4.19$ for the $B(M1)$.

The output of the shell-model calculations regarding the level and decay scheme can be seen in the left part of Fig. 4. The three lowest excited states (2_1^+, 4_1^+, 6_1^+) are known from previous studies and can be unambiguously connected to the experimental levels. The calculation also provides four states (2_2^+, 4_2^+, 5_2^+, 6_2^+) associated with mainly neutron excitations not populated by $(p, 2p)$ reaction in the experiment. However, the wave function of the colored (green for 4_3^+, brown for 5_1^+, cyan for 6_3^+) states shows dominance of proton excitations in Table I (mainly $f_{7/2} \rightarrow f_{5/2}$) which are generally accessible by our experimental probe. This means that the shell model provides good candidates for our experimental proton hole states in the energy range 3.5–4.1 MeV. According to the calculations, the 6_3^+ state essentially decays to the 6_1^+ state. The 6_1^+ state decays to the 4_1^+ state by emitting a γ ray of 355 keV. Considering the calculated $B(E2)$, the partial half-life for the 355 keV photon emission is 1.8 ns, which would imply a smeared but visible peak around 300–350 keV in the experimental spectrum. Also, in this case the $4_1^+ \rightarrow 2_1^+$ and the $2_1^+ \rightarrow 0_1^+$ transitions would include a long-lived component, which can be excluded from their lineshape. Therefore, probably none of our experimental states should correspond to the 6_3^+ state. Both of the 5_1^+ and 4_3^+ states decay to the 4_1^+ state. Thus, they are good candidates for the experimental 4147 keV level. However, the calculation suggests significant decay to the 6_1^+ state from the 5_1^+ state and to the 2_1^+ state from the 4_3^+ state, which would results in strong γ rays of 355 and 1872 keV for the first case and a significant γ ray of 3157 keV for the second case. Our simulations show that the upper limits on the number of counts for either the $5_1^+ \rightarrow 6_1^+$ or the $4_3^+ \rightarrow 2_1^+$ transitions would make them at most 20% branches not as significant as in the theoretical calculations.

To compare the deduced exclusive cross sections for the proton hole states, we calculated the single-particle cross

TABLE II. Theoretical level energies (E_{theor}), spectroscopic factors, $(p, 2p)$ exclusive cross sections (σ_{theor}) together with experimental level energies (E_{expt}) and cross sections (σ_{expt}). The level energies and the spectroscopic factors originate from our shell-model calculations while the cross sections were derived by combining DWIA cross sections and the spectroscopic factors. The uncertainty in the DWIA framework and its input is about 20% as discussed in Ref. [42]. Above 4 MeV, only those excited states are shown for which the theoretical cross section exceeds 0.1 mb. Regarding the experimental data, only the first four states could be unambiguously assigned to theoretical levels. The experimental 4147 keV state and the corresponding experimental $(p, 2p)$ cross section is shown together with the theoretical 4_3^+ level; however, the 4147 keV state may also belong to the theoretical 5_1^+ level.

E_{theor} (MeV)	J^π	Spectroscopic factor		σ_{theor} (mb)	E_{expt} (MeV)	σ_{expt} (mb)
0	0_1^+	0.60	$f_{5/2}$	0.74	0	$\leqslant$6.9
0.846	2_1^+	<0.01	$f_{7/2}$	0.28	0.990	$\leqslant$0.57
		0.23	$f_{5/2}$			
2.038	4_1^+	<0.01	$f_{7/2}$	<0.10	1.920	$\leqslant$0.68
		<0.01	$f_{5/2}$			
2.913	6_1^+	<0.01	$f_{7/2}$	<0.10	2.275	
					3.431	0.65(33)
					3.828	0.38(16)
3.550	4_3^+	0.77	$f_{7/2}$	1.08	4.147	1.17(25)
		<0.01	$f_{5/2}$			
3.603	5_1^+	0.72	$f_{7/2}$	1.02		
		<0.01	$f_{5/2}$			
4.164	6_3^+	0.62	$f_{7/2}$	0.86		
3.046	2_2^+	<0.01	$f_{7/2}$	<0.10		
		<0.01	$f_{5/2}$			
3.393	4_2^+	0.11	$f_{7/2}$	0.15		
		<0.01	$f_{5/2}$			
3.727	5_2^+	0.03	$f_{7/2}$	<0.10		
		<0.01	$f_{5/2}$			
4.007	6_2^+	0.23	$f_{7/2}$	0.31		
4.468	4_5^+	0.09	$f_{7/2}$	0.13		
		<0.01	$f_{5/2}$			
4.862	6_4^+	0.09	$f_{7/2}$	0.12		
4.900	4_8^+	0.08	$f_{7/2}$	0.11		
		<0.01	$f_{5/2}$			
4.970	2_7^+	<0.01	$f_{7/2}$	0.51		
		0.37	$f_{5/2}$			
5.106	6_5^+	0.28	$f_{7/2}$	0.38		
5.243	6_6^+	0.08	$f_{7/2}$	0.10		
5.352	5_7^+	0.14	$f_{7/2}$	0.18		
		<0.01	$f_{5/2}$			
5.409	2_9^+	<0.01	$f_{7/2}$	0.14		
		0.10	$f_{5/2}$			

sections for the $(p, 2p)$ reaction by integrating the differential cross section of the distorted-wave impulse approximation (DWIA) framework given in Eq. (3.52) of Ref. [42] over E_1^{L}, Ω_1^{L}, Ω_2^{L}, and divided by two. The single-particle wave function and the nuclear density were obtained by the Bohr–Mottelson single-particle potential [43]. The optical potentials for the distorted waves in the initial and final channels were constructed by the microscopic folding model [44] with the Melbourne g-matrix interaction [45] and the calculated nuclear density. The spin-orbit part of each distorting potential was disregarded. As for the pp interaction, the Franey–Love effective interaction [46] was adopted. These theoretical cross sections were combined with the spectroscopic factors of our shell-model calculations and averaged over the beam energy covered by our target similar to the experimental exclusive cross sections. The resulting theoretical cross sections for the relevant states are listed in Table II. If we add the cross sections up to the estimated neutron separation energy of 5.4 MeV for ^{76}Ni [47] taking into account knock-out from $f_7/2$ and $f_5/2$ single-particle states, we end up with 7.4 mb. This value is very close to our experimental inclusive cross section of 8.4(4) mb. Furthermore, the calculated exclusive cross sections for the 2_1^+, 4_1^+, and 6_1^+ states are consistent with the experimental findings. The theoretical cross sections for the 4_3^+, 5_1^+, and 6_3^+ states are 1.08, 1.02, and 0.86 mb, respectively. These values are comparable to our experimental cross sections for the proton hole states (3431, 3828, 4147 keV) indicated in Fig. 4. All in all, a good agreement was achieved between the experimental and the theoretical cross sections taking into account the uncertainties. It must be noted, however, that a small value of 0.74 mb was calculated for the ground state while we could give a much higher experimental upper limit. This indicates that some excited states may remain unobserved due to the modest resolution of the DALI2 array.

Although further theoretical efforts are needed to fully understand the experimental data, our results shows consistency with a strong proton shell closure for nickel isotopes since the employed shell-model interaction assumes a proton gap of 5.2 MeV, a value compatible with the most recent theoretical and experimental studies in the region [22,48].

IV. SUMMARY

The low-energy level structure of ^{76}Ni nucleus was investigated by proton knock-out reactions. The γ spectroscopy study in the ^{77}Cu$(p, 2p)^{76}$Ni channel revealed three new transitions with energies of 2227, 2441, and 2838 keV. The $\gamma\gamma$ and $\gamma\gamma\gamma$ coincidence spectra showed that the first γ ray was in coincidence with both the known 930 and 990 keV transitions of the $4_1^+ \rightarrow 2_1^+ \rightarrow 0_1^+$ cascade. This established a new excited state at 4147 keV. The two other new transitions could be tentatively placed feeding the 2_1^+ state, which implied two possible new states at 3431 and 3828 keV. Comparing the experimental results to shell-model calculations, the experimental state at 4147 keV could be assigned to either the 5_1^+ or the 4_3^+ theoretical proton hole states. Besides, the calculated cross sections agree quite well with the experimental ones, and our results suggest a substantial $Z = 28$ shell closure in the region.

ACKNOWLEDGMENTS

The authors are thankful to the RIBF and BigRIPS teams for the stable operation and high intensity of the uranium primary beam, and production of secondary beams during the experiment. The development of MINOS and the core MINOS team have been supported by the European Research Council through the ERC Grant No. MINOS-258567. A.O. was supported by JSPS long-term fellowship L-13520 from September 2013 to June 2014 at the RIKEN Nishina Center. A.O. deeply thanks the ERC and JSPS for their support. C.S. was supported by the IPA program at the RIKEN Nishina Center. A.O. and C.S. are grateful to the RIKEN Nishina Center for its hospitality. This work was supported by JSPS Grant-in-Aid for a JSPS Research Fellow (No. 268718). Z.E. was supported by the NKFIH-NN114454 contract and Á.K. by ÚNKP program of the Ministry of Human Capacities. L.X.C. would like to thank MOST for its support through the Physics Development Program Grant No. ĐTĐLCN.25/18. M.L. and V.W. acknowledge the German BMBF with the supporting No. 05P15RDFN1 and No. 05P12RDFN8. D.S. and Zs.D. were partly supported by the GINOP-2.3.3-15-2016-00034 contract. K.O. acknowledges the support by Grant-in-Aid for Scientific Research JP16K05352.

[1] M. G. Mayer, Phys. Rev. **74**, 235 (1948).
[2] M. G. Mayer, Phys. Rev. **75**, 1969 (1949).
[3] Z. Dombrádi, Z. Elekes, A. Saito, N. Aoi, H. Baba, K. Demichi, Z. Fülöp, J. Gibelin, T. Gomi, H. Hasegawa *et al.*, Phys. Rev. Lett. **96**, 182501 (2006).
[4] A. Gade, D. Bazin, B. A. Brown, C. M. Campbell, J. M. Cook, S. Ettenauer, T. Glasmacher, K. W. Kemper, S. McDaniel, A. Obertelli *et al.*, Phys. Rev. C **83**, 044305 (2011).
[5] M. Seidlitz, P. Reiter, R. Altenkirch, B. Bastin, C. Bauer, A. Blazhev, N. Bree, B. Bruyneel, P. A. Butler, J. Cederkäll *et al.*, Phys. Rev. C **89**, 024309 (2014).
[6] P. Doornenbal, H. Scheit, S. Takeuchi, Y. Utsuno, N. Aoi, K. Li, M. Matsushita, D. Steppenbeck, H. Wang, H. Baba *et al.*, Phys. Rev. C **95**, 041301 (2017).
[7] B. Fernández-Domínguez, B. Pietras, W. Catford, N. Orr, M. Petri, M. Chartier, S. Paschalis, N. Patterson, J. Thomas, M. Caamano *et al.*, Phys. Lett. B **779**, 124 (2018).
[8] B. Bastin, S. Grévy, D. Sohler, O. Sorlin, Z. Dombrádi, N. L. Achouri, J. C. Angélique, F. Azaiez, D. Baiborodin, R. Borcea *et al.*, Phys. Rev. Lett. **99**, 022503 (2007).
[9] S. Takeuchi, T. Motobayashi, Y. Togano, M. Matsushita, N. Aoi, K. Demichi, H. Hasegawa, and H. Murakami, Nucl. Instrum. Methods Phys. Res., Sect. A **763**, 596 (2014).
[10] D. T. Tran, H. J. Ong, G. Hagen, T. D. Morris, N. Aoi, T. Suzuki, Y. Kanada-En'yo, L. S. Geng, S. Terashima, I. Tanihata *et al.*, Nat. Commun. **9**, 1594 (2018).

[11] Y. Togano, Y. Yamada, N. Iwasa, K. Yamada, T. Motobayashi, N. Aoi, H. Baba, S. Bishop, X. Cai, P. Doornenbal *et al.*, Phys. Rev. Lett. **108**, 222501 (2012).
[12] Y. Utsuno, T. Otsuka, T. Mizusaki, and M. Honma, Phys. Rev. C **60**, 054315 (1999).
[13] T. Otsuka, R. Fujimoto, Y. Utsuno, B. A. Brown, M. Honma, and T. Mizusaki, Phys. Rev. Lett. **87**, 082502 (2001).
[14] T. Otsuka, T. Matsuo, and D. Abe, Phys. Rev. Lett. **97**, 162501 (2006).
[15] T. Otsuka, T. Suzuki, M. Honma, Y. Utsuno, N. Tsunoda, K. Tsukiyama, and M. Hjorth-Jensen, Phys. Rev. Lett. **104**, 012501 (2010).
[16] K. Sieja and F. Nowacki, Phys. Rev. C **81**, 061303 (2010).
[17] K. Sieja and F. Nowacki, Phys. Rev. C **85**, 051301 (2012).
[18] C. Mazzocchi, R. Grzywacz, J. Batchelder, C. Bingham, D. Fong, J. Hamilton, J. Hwang, M. Karny, W. Krolas, S. Liddick *et al.*, Phys. Lett. B **622**, 45 (2005).
[19] P. Hosmer, H. Schatz, A. Aprahamian, O. Arndt, R. R. C. Clement, A. Estrade, K. Farouqi, K.-L. Kratz, S. N. Liddick, A. F. Lisetskiy *et al.*, Phys. Rev. C **82**, 025806 (2010).
[20] Z. Y. Xu, S. Nishimura, G. Lorusso, F. Browne, P. Doornenbal, G. Gey, H.-S. Jung, Z. Li, M. Niikura, P.-A. Söderström *et al.*, Phys. Rev. Lett. **113**, 032505 (2014).
[21] C. Santamaria, C. Louchart, A. Obertelli, V. Werner, P. Doornenbal, F. Nowacki, G. Authelet, H. Baba, D. Calvet, F. Château *et al.*, Phys. Rev. Lett. **115**, 192501 (2015).
[22] L. Olivier, S. Franchoo, M. Niikura, Z. Vajta, D. Sohler, P. Doornenbal, A. Obertelli, Y. Tsunoda, T. Otsuka, G. Authelet *et al.*, Phys. Rev. Lett. **119**, 192501 (2017).
[23] M. L. Cortés, P. Doornenbal, M. Dupuis, S. M. Lenzi, F. Nowacki, A. Obertelli, S. Péru, N. Pietralla, V. Werner, K. Wimmer *et al.*, Phys. Rev. C **97**, 044315 (2018).
[24] Z. Vajta, D. Sohler, Y. Shiga, K. Yoneda, K. Sieja, D. Steppenbeck, Z. Dombrádi, N. Aoi, P. Doornenbal, J. Lee *et al.*, Phys. Lett. B **782**, 99 (2018).
[25] P.-A. Söderström, S. Nishimura, Z. Y. Xu, K. Sieja, V. Werner, P. Doornenbal, G. Lorusso, F. Browne, G. Gey, H. S. Jung *et al.*, Phys. Rev. C **92**, 051305 (2015).
[26] T. Kubo, D. Kameda, H. Suzuki, N. Fukuda, H. Takeda, Y. Yanagisawa, M. Ohtake, K. Kusaka, K. Yoshida, N. Inabe *et al.*, Prog. Theor. Exp. Phys. **2012**, 03C003 (2012).
[27] N. Fukuda, T. Kubo, T. Ohnishi, N. Inabe, H. Takeda, D. Kameda, and H. Suzuki, Nucl. Instrum. Methods Phys. Res., Sect. B **317**, 323 (2013).
[28] K. Kimura, T. Izumikawa, R. Koyama, T. Ohnishi, T. Ohtsubo, A. Ozawa, W. Shinozaki, T. Suzuki, M. Takahashi, I. Tanihata *et al.*, Nucl. Instrum. Methods Phys. Res., Sect. A **538**, 608 (2005).
[29] H. Kumagai, A. Ozawa, N. Fukuda, K. Sümmerer, and I. Tanihata, Nucl. Instrum. Methods Phys. Res., Sect. A **470**, 562 (2001).
[30] H. Kumagai, T. Ohnishi, N. Fukuda, H. Takeda, D. Kameda, N. Inabe, K. Yoshida, and T. Kubo, Nucl. Instrum. Methods Phys. Res., Sect. B **317**, 717 (2013).
[31] A. Obertelli, A. Delbart, S. Anvar, L. Audirac, G. Authelet, H. Baba, B. Bruyneel, D. Calvet, F. Château, A. Corsi *et al.*, Eur. Phys. J. A **50**, 8 (2014).
[32] C. Santamaria, Quest for new nuclear magic numbers with MINOS, Ph.D. thesis, Université Paris Sud - Paris XI, 2015.
[33] D. Kameda, T. Kubo, T. Ohnishi, K. Kusaka, A. Yoshida, K. Yoshida, M. Ohtake, N. Fukuda, H. Takeda, K. Tanaka *et al.*, Phys. Rev. C **86**, 054319 (2012).
[34] M. M. Rajabali, R. Grzywacz, S. N. Liddick, C. Mazzocchi, J. C. Batchelder, T. Baumann, C. R. Bingham, I. G. Darby, T. N. Ginter, S. V. Ilyushkin *et al.*, J. Phys. G **41**, 115104 (2014).
[35] S. Agostinelli, J. Allison, K. Amako, J. Apostolakis, H. Araujo, P. Arce, M. Asai, D. Axen, S. Banerjee, G. Barrand *et al.*, Nucl. Instrum. Methods Phys. Res., Sect. A **506**, 250 (2003).
[36] S. M. Lenzi, F. Nowacki, A. Poves, and K. Sieja, Phys. Rev. C **82**, 054301 (2010).
[37] P. Morfouace, S. Franchoo, K. Sieja, I. Matea, L. Nalpas, M. Niikura, A. Sánchez-Benítez, I. Stefan, M. Assié, F. Azaiez *et al.*, Phys. Lett. B **751**, 306 (2015).
[38] E. Sahin, M. Doncel, K. Sieja, G. de Angelis, A. Gadea, B. Quintana, A. Görgen, V. Modamio, D. Mengoni, J. J. Valiente-Dobón *et al.*, Phys. Rev. C **91**, 034302 (2015).
[39] P. Morfouace, S. Franchoo, K. Sieja, I. Stefan, N. de Séréville, F. Hammache, M. Assié, F. Azaiez, C. Borcea, R. Borcea *et al.*, Phys. Rev. C **93**, 064308 (2016).
[40] F. Nowacki and E. Caurier, Acta Phys. Pol. B **30**, 749 (1999).
[41] E. Caurier, G. Martínez-Pinedo, F. Nowacki, A. Poves, and A. P. Zuker, Rev. Mod. Phys. **77**, 427 (2005).
[42] T. Wakasa, K. Ogata, and T. Noro, Prog. Part. Nucl. Phys. **96**, 32 (2017).
[43] A. Bohr and B. Mottelson, *Nuclear Structure* (Benjamin, New York, 1969), Vol. I.
[44] M. Toyokawa, K. Minomo, and M. Yahiro, Phys. Rev. C **88**, 054602 (2013).
[45] K. Amos, P. Dortmans, H. von Geramb, S. Karataglidis, and J. Raynal, Adv. Nucl. Phys. **25**, 275 (2000).
[46] M. A. Franey and W. G. Love, Phys. Rev. C **31**, 488 (1985).
[47] M. Wang, G. Audi, F. Kondev, W. Huang, S. Naimi, and X. Xu, Chin. Phys. C **41**, 030003 (2017).
[48] F. Nowacki, A. Poves, E. Caurier, and B. Bounthong, Phys. Rev. Lett. **117**, 272501 (2016).